I. SUPPLEMENTAL FIGURES AND MOVIES

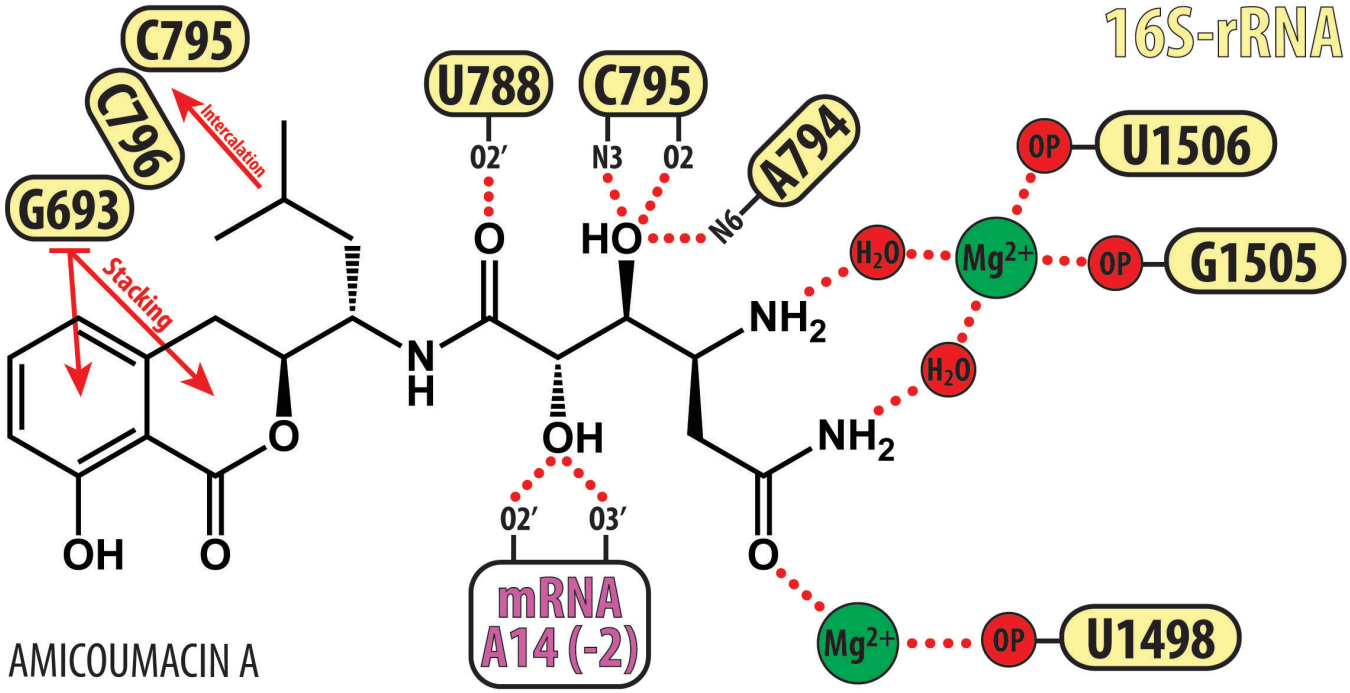

Figure S1, related to Figure 2. Schematic overview of AMI interactions on the ribosome. Nucleotides of the 16S rRNA are highlighted light yellow, mRNA is magenta. H-bonds and coordination bonds are shown as red dots. Hydrophobic interactions, such as stacking or intercalation, are displayed as red arrows. Non-bridging phosphate oxygens (OP) and magnesium-coordinated waters are colored red, while magnesium ions are shown green.

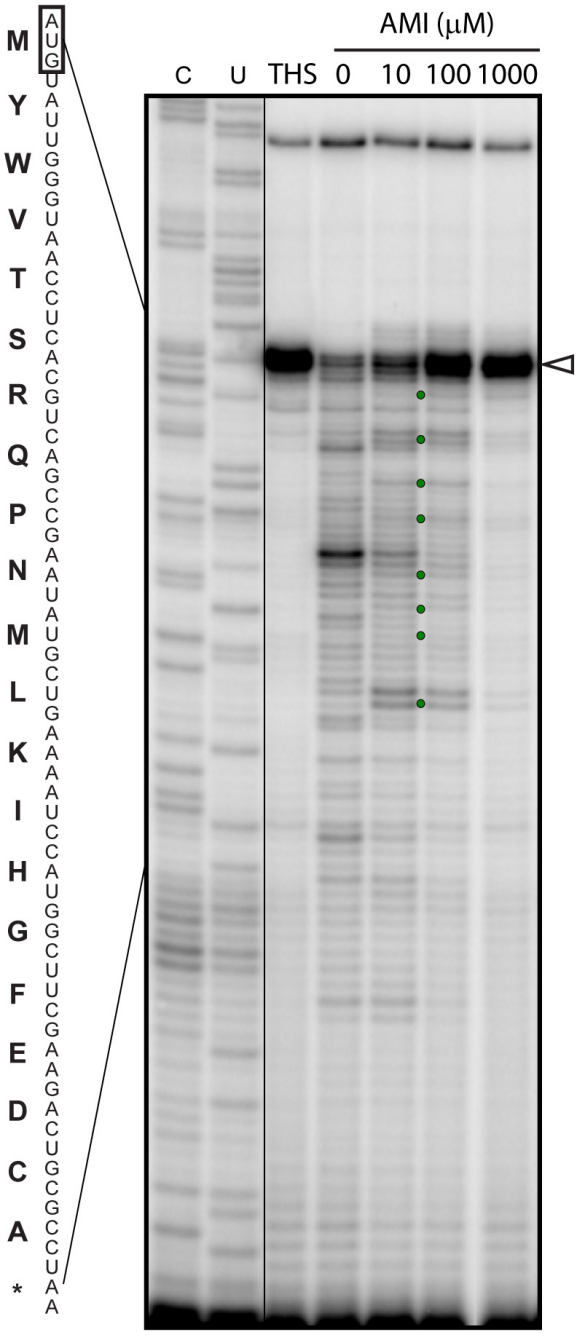

Figure S2, related to Figure 3. AMI is an elongation inhibitor that can act past initiation. Toe-printing analysis of translation of the synthetic 21-codon mRNA RST1 (Orelle et al., 2013) in the presence of increasing concentrations of AMI. Thiostrepton (THS), added to the reaction at 50 mM concentration, arrests the ribosome at the initiator codon (the corresponding toe-printing band is indicated by a white triangle). The toe-printing bands, which appear at lower concentrations of AMI and which reflect inhibition of translation elongation by AMI at the internal codons of the *RST1* gene, are indicated by green dots.

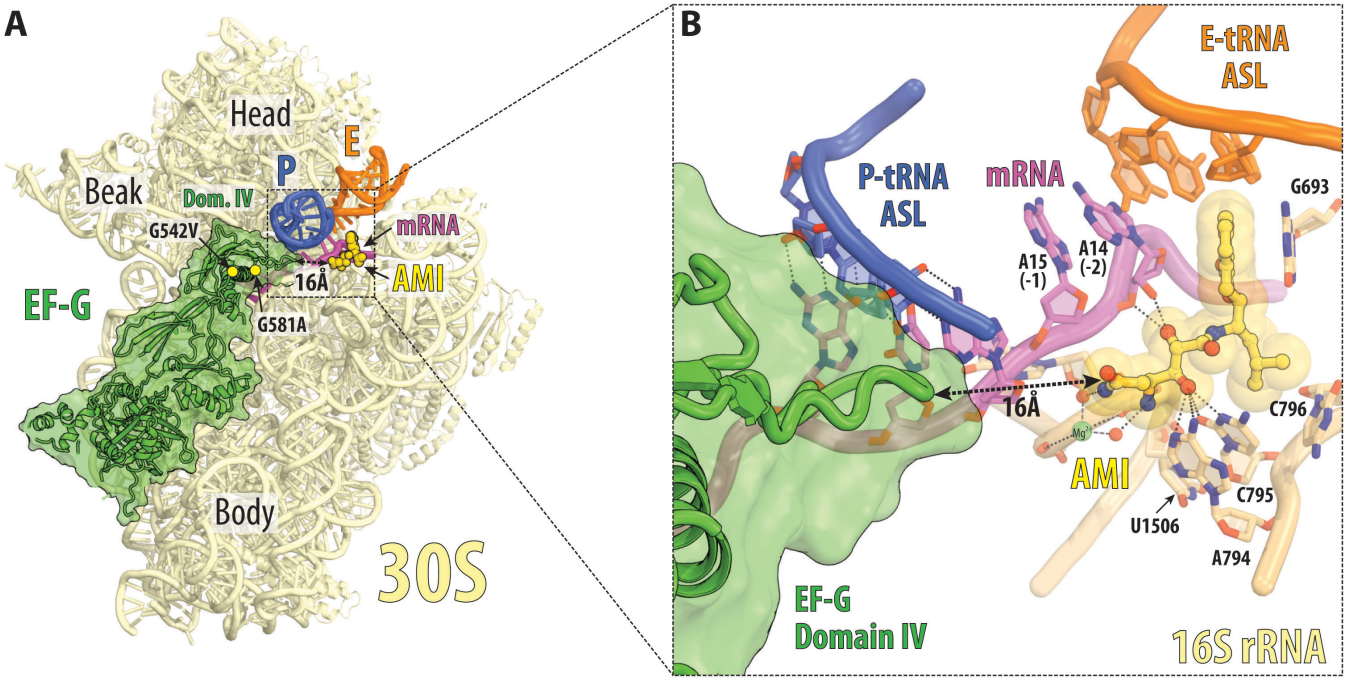

Figure S3, related to Figure 3. Superposition of 70S-AMI structure with the ribosome-bound EF-G. (**A**) Overview and (**B**) close-up view of the structure of AMI (yellow) in complex with the *T. thermophilus* 70S ribosome superimposed with the structure of ribosome-bound EF-G (green) (PDB entry 2WRI (Gao et al., 2009)). Superposition is based on the alignment of 16S rRNA. The 30S subunit (light yellow) is viewed from the intersubunit interface (50S subunit is removed for clarity). The mRNA is shown in magenta and tRNAs are displayed in dark blue for the P-site, and in orange for the E-site. Only the anticodon stems of tRNAs are shown. The shortest distance between AMI and the tip of domain IV of EF-G is indicated by dashed arrow. Two mutations G542V and G581A in the domain IV of EF-G which confer resistance to AMI are indicated by yellow circles. The shortest distances from the Cα-atoms of the residues V542 and A581 to AMI are 38Å and 30Å, respectively.

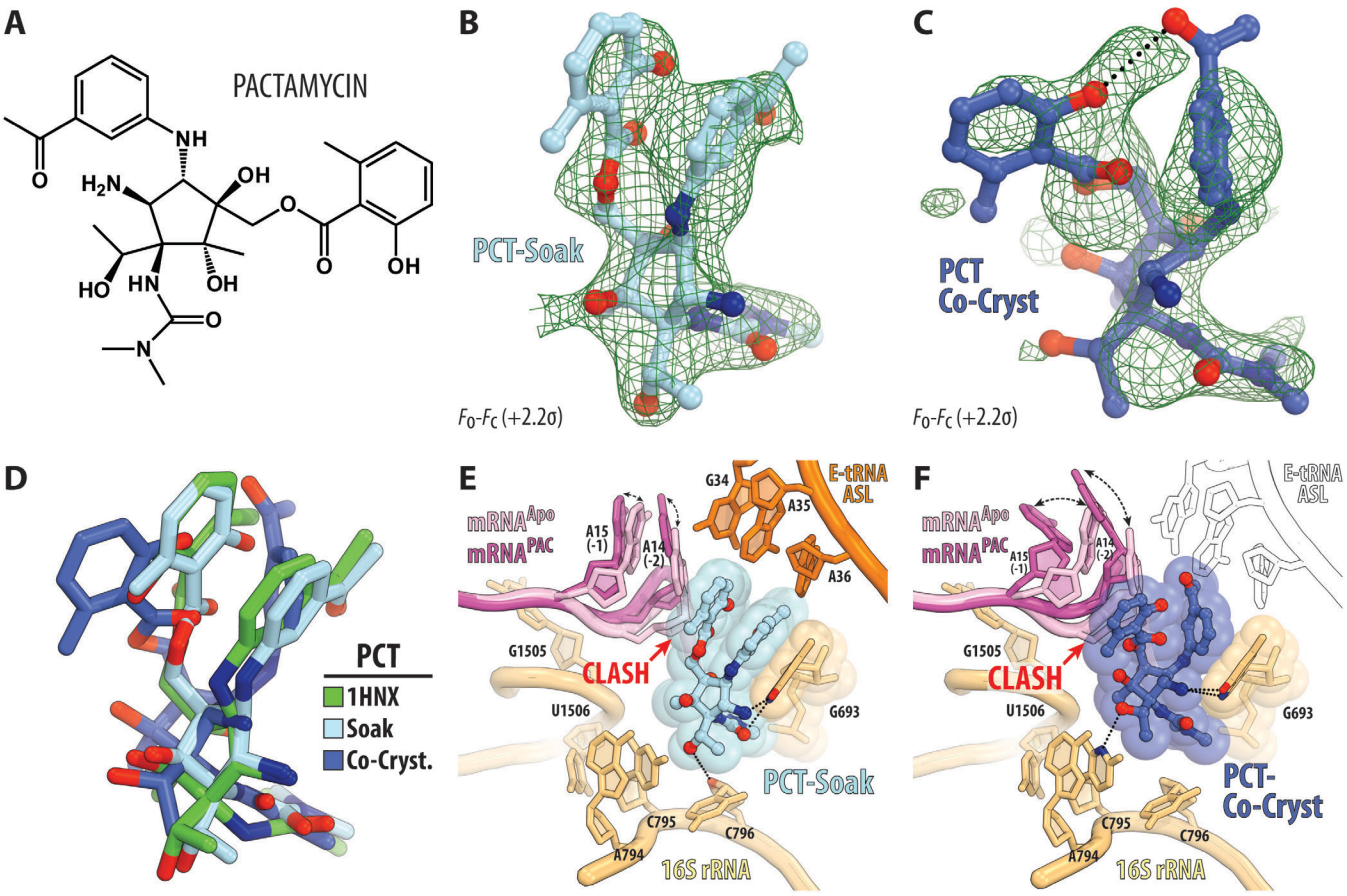

Figure S4, related to Figure 4. Binding of PCT to the 70S ribosome. (**A**) Chemical structure of pactamycin. (**B**, **C**) Unbiassed (F_{obs} – F_{calc}) difference Fourier maps of PCT in complex with the *T. thermophilus* 70S ribosome contoured at 2.2 σ. PCT is colored in light blue for the soaking experiment and in dark blue for the co-crystallization experiment. Nitrogens are colored blue, oxygens are colored red. (**D**) Comparison of the superimposed structures of PCT. The previously published structure of PCT in complex with only the 30S ribosomal subunit is shown in green (PDB entry 1HNX (Brodersen et al., 2000)). The structure of PCT from the current work in complex with the 70S ribosome from the soaking experiment is in light blue and from the co-crystallization experiment is in dark-blue. All structures were aligned based on h24 of the 16S rRNA (nucleotides 769-810). (**E**, **F**) Close-up views of the PCT binding site on the *T. thermophilus* 70S ribosome. The coloring of PCT is the same as in (D). The 16S rRNA is shown in light yellow, mRNA is in magenta, and the anticodon stem loop (ASL) of the E-site tRNA is in orange. The typical location of the mRNA in the absence of cognate tRNA in the E site is shown in pink as reference. The black contour of the E-site tRNA in (F) indicates that it is absent from the structure. Steric clashes between the antibiotic and parts of the ribosome are indicated by red arrows. Note, that binding of PCT to the ribosome causes displacement of the mRNA from its normal

location (dashed arrows). Also note, that co-crystallization and soaking experiments yielded non-identical orientations of PCT in its binding site on the small ribosomal subunit. See also Movie S2.

Movie S1, related to Figure 2. AMI functional site in the 70S ribosome. The movie shows: (1) zoom-out and (2) close-up views of the AMI binding site in the small subunit of the *T. thermophilus* 70S ribosome programmed with mRNA and three tRNAs; (3) details of AMI interactions with the mRNA and 16S rRNA in the E site of the ribosome shown in three different perspectives.

Movie S2, related to Figures 4 and S4. Conformational flexibility of PCT bound to the 70S ribosome. The movie shows: (1) zoom-out and close-up views of the PCT binding site in the small subunit of the *T. thermophilus* 70S ribosome programmed with mRNA and three tRNAs, highlighting details of PCT interactions with the 16S rRNA; (2) morph between the structure of the vacant ribosome and the structure of the ribosome with PCT in the compact conformation (PCT soaking experiment) illustrating how steric clash between PCT and the mRNA in the ribosomal E site can cause partial mRNA displacement; (3) morph between the compact and the extended conformations of PCT (co-crystallization experiment) illustrating how more severe steric clash between PCT and mRNA can further displace the mRNA, break the stacking interactions between mRNA and the E-site tRNA and lead eventually to dissociation of the tRNA from the E site.

II. SUPPLEMENTAL EXPERIMENTAL PROCEDURES

1. Purification of *T. thermophilus* 70S ribosomes

T.thermophilus 70S ribosomes were prepared as described previously (Selmer et al., 2006). The final 70S pellets were resuspended at a concentration of approximately 500 A_{260} units/ml in a buffer containing 5 mM HEPES-KOH (pH 7.6), 50 mM KCl, 10 mM NH_4Cl, 10 mM $Mg(CH_3COO)_2$, 6 mM β-mercaptoethanol, flash frozen in liquid nitrogen and stored in small aliquots at -80°C until used in crystallization experiments.

2. Preparation of mRNA and tRNAs

Synthetic mRNA with the sequence 5'-GGC AAG GAG GUA AAA AUG UUC UAA-3' was obtained from Integrated DNA Technologies (Coralville, IA). This mRNA includes a Shine-Dalgarno sequence, an AUG start codon (red) and a phenylalanine UUC codon (blue) followed by a stop codon. Unmodified *E.coli* tRNAs were overexpressed and purified as described previously for $tRNA_i^{Met}$ (Schmitt et al., 1999) and for $tRNA^{Phe}$ (Junemann et al., 1996).

3. Complex formation

Ribosome-mRNA-tRNA complexes were formed by programming of 5 μM 70S *T. thermophilus* ribosomes with 10 μM mRNA and incubation at 55°C for 10 minutes, followed by addition of 20 μM P- and A-site tRNA substrates (with minor changes from (Voorhees et al., 2009)). Each of the last two steps was allowed to reach equilibrium for 10 minutes at 37°C. In the co-crystallization experiments with PCT (Sigma), the antibiotic was added to a final concentration of 100 μM and the complex was left at room temperature for an additional 15 minutes prior to crystallization. For soaking experiments with either AMI or PCT, the antibiotics were not added at this point, and, instead, were included into the crystal-stabilization solutions at a later step. The programmed 70S ribosomes were crystallized in the buffer containing 5 mM HEPES-KOH (pH 7.6), 50 mM KCl, 10 mM NH_4Cl and 10 mM $Mg(CH_3COO)_2$.

4. Crystallization

Initial crystalline needles were obtained by screening around previously published ribosome crystallization conditions (Korostelev et al., 2006; Polikanov et al., 2012; Selmer et al., 2006). Crystals were grown by vapor diffusion in sitting drop crystallization trays at 19°C. 2-3 μL of the 70S ribosome complexes were mixed with 3-4 μL of a reservoir solution containing 100 mM Tris-HCl (pH 7.6), 2.9% (w/v) PEG-20K, 7-12% (v/v) MPD, 100-200 mM arginine, 0.5 mM β-mercaptoethanol. Crystals appeared within 2-3 days and grew up to 200 × 200 × 1500 μm in size within 7-8 days. Crystals were cryo-protected stepwise using a series of buffers with increasing MPD concentrations until reaching a final concentration of 40% (v/v) MPD, at which point they were incubated overnight at 19°C. In

addition to MPD, all stabilization buffers contained 100 mM Tris-HCl (pH 7.6), 2.9% (w/v) PEG-20K, 50 mM KCl, 10 mM NH_4Cl, 10 mM Mg_2Cl, and 6 mM β-mercaptoethanol. The final stabilization buffer (40% MPD) also contained either 250 μM AMI or 100 μM PCT. After stabilization, crystals were harvested and immediately flash frozen in a nitrogen cryo-stream at 80K.

5. Data Collection and Processing

Diffraction data were collected using beamline 24ID-C at the Advanced Photon Source (Argonne, IL) and beamline X25 at the Brookhaven National Laboratory (Upton, NY). A complete dataset for each ribosome complex was collected at 100K from multiple regions of the same crystal using 0.2° oscillations. The raw data were integrated and scaled using the XDS software package (Kabsch, 2010). All of the crystals belonged to the primitive orthorhombic space group $P2_12_12_1$ with approximate unit cell dimensions of 210Å × 450Å × 620Å and contained two copies of the 70S ribosome per asymmetric unit (Table S1). Each structure was solved by molecular replacement using PHASER from the CCP4 program suite (McCoy et al., 2007). The search model was generated from the previously published structure of *T. thermophilus* 70S ribosome with bound mRNA and tRNAs (PDB entries 4QCM, 4QCN (Polikanov et al., 2014)). Coordinates for AMI or PCT were excluded from the starting search model. The initial molecular replacement solutions were refined with the ribosome split into multiple rigid-body domains, followed by 7 cycles of positional and individual B-factor refinement using PHENIX (Adams et al., 2010). Non-crystallographic symmetry restraints were applied to 4 domains of the 30S ribosomal subunit (head, body, spur, helix 44), and 3 domains of the 50S subunit (body, L1-stalk, N-terminus of the L9 protein). After initial refinement, electron density corresponding to AMI or PCT became evident in the unbiased F_o–F_c difference maps.

6. Model Building

Atomic models of AMI and PCT were generated from their known chemical structures using PRODRG online software (Schuttelkopf and van Aalten, 2004), which was also used to generate restraints based on idealized 3D geometry. Atomic model and restraints were used to fit/refine AMI or PCT into the obtained unbiased electron densities.

The final model for 70S ribosome in complex with either AMI or PCT was generated by multiple rounds of model building in COOT (Emsley and Cowtan, 2004), followed by refinement in PHENIX (Adams et al., 2010). The statistics of data collection and refinement for each complex are compiled in Table S1.

The 1.0-1.2 Å increase in resolution achieved over existing structures of 70S complexes enabled us to build a more complete and accurate model of the 70S ribosome than in previous structures. The markedly improved overall quality of the electron density maps allowed us to rectify some main-chain

register problems and to improve the number of residues falling into the favored and allowed regions of the Ramachandran plot for many ribosomal proteins in our starting model.

7. Figures and movies

All figures and movies showing atomic models were generated using PYMOL (www.pymol.org).

III. SUPPLEMENTAL REFERENCES

Adams, P.D., Afonine, P.V., Bunkoczi, G., Chen, V.B., Davis, I.W., Echols, N., Headd, J.J., Hung, L.W., Kapral, G.J., Grosse-Kunstleve, R.W., *et al.* (2010). PHENIX: a comprehensive Python-based system for macromolecular structure solution. Acta Crystallogr. D Biol. Crystallogr. *66*, 213-221.

Brodersen, D.E., Clemons, W.M., Jr., Carter, A.P., Morgan-Warren, R.J., Wimberly, B.T., and Ramakrishnan, V. (2000). The structural basis for the action of the antibiotics tetracycline, pactamycin, and hygromycin B on the 30S ribosomal subunit. Cell *103*, 1143-1154.

Emsley, P., and Cowtan, K. (2004). Coot: model-building tools for molecular graphics. Acta Crystallogr. D Biol. Crystallogr. *60*, 2126-2132.

Gao, Y.G., Selmer, M., Dunham, C.M., Weixlbaumer, A., Kelley, A.C., and Ramakrishnan, V. (2009). The structure of the ribosome with elongation factor G trapped in the posttranslocational state. Science *326*, 694-699.

Junemann, R., Wadzack, J., Triana-Alonso, F.J., Bittner, J.U., Caillet, J., Meinnel, T., Vanatalu, K., and Nierhaus, K.H. (1996). In vivo deuteration of transfer RNAs: overexpression and large-scale purification of deuterated specific tRNAs. Nucleic. Acids Res. *24*, 907-913.

Kabsch, W. (2010). Xds. Acta Crystallogr. D Biol. Crystallogr. *66*, 125-132.

Korostelev, A., Trakhanov, S., Laurberg, M., and Noller, H.F. (2006). Crystal structure of a 70S ribosome-tRNA complex reveals functional interactions and rearrangements. Cell *126*, 1065-1077.

McCoy, A.J., Grosse-Kunstleve, R.W., Adams, P.D., Winn, M.D., Storoni, L.C., and Read, R.J. (2007). Phaser crystallographic software. J. Appl. Crystallogr. *40*, 658-674.

Orelle, C., Szal, T., Klepacki, D., Shaw, K.J., Vazquez-Laslop, N., and Mankin, A.S. (2013). Identifying the targets of aminoacyl-tRNA synthetase inhibitors by primer extension inhibition. Nucleic Acids Res. *41*, e144.

Polikanov, Y.S., Blaha, G.M., and Steitz, T.A. (2012). How hibernation factors RMF, HPF, and YfiA turn off protein synthesis. Science *336*, 915-918.

Polikanov, Y.S., Steitz, T.A., and Innis, C.A. (2014). A proton wire to couple aminoacyl-tRNA accommodation and peptide bond formation on the ribosome. Nat. Struct. Mol. Biol. *21*, 787-793.

Schmitt, E., Blanquet, S., and Mechulam, Y. (1999). Crystallization and preliminary X-ray analysis of Escherichia coli methionyl-tRNAMet(f) formyltransferase complexed with formyl-methionyl-tRNAMet(f). Acta Crystallogr. D Biol. Crystallogr. *55*, 332-334.

Schuttelkopf, A.W., and van Aalten, D.M. (2004). PRODRG: a tool for high-throughput crystallography of protein-ligand complexes. Acta Crystallogr. D Biol. Crystallogr. *60*, 1355-1363.

Selmer, M., Dunham, C.M., Murphy, F.V.t., Weixlbaumer, A., Petry, S., Kelley, A.C., Weir, J.R., and Ramakrishnan, V. (2006). Structure of the 70S ribosome complexed with mRNA and tRNA. Science *313*, 1935-1942.

Voorhees, R.M., Weixlbaumer, A., Loakes, D., Kelley, A.C., and Ramakrishnan, V. (2009). Insights into substrate stabilization from snapshots of the peptidyl transferase center of the intact 70S ribosome. Nat. Struct. Mol. Biol. *16*, 528-533.